IRAQI JOURNAL OF MATERIALS
Volume (5) Issue (1) January-March 2026, pp. 25-30
Published and Sponsored by American Quality for Scientific Publishing, Inc. (AQSP)

Particle Size-Dependent Energy Conversion in Plasmonic Nanostructures for Photothermal Catalysis Applications

Abdullah M. Alsaedi*, Majed N. Odah

Department of Physics, College of Science, University of Basrah, Basrah, IRAQ
Corresponding author email: abdullah2311975@yahoo.com

Abstract
This work examines the influence of nanoparticle size and morphology on the photothermal catalytic behavior of gold and silver nanostructures. Localized surface plasmon resonance (LSPR) effects were tuned to optimize light absorption and heat generation. A tight and nonlinear relation between particle diameter and optical properties was confirmed as the particles with diameters in the range 25-35 nm have achieved the maximum efficiency of light absorption, making this range optimum to convert the photons into condensed local heat. A radical transformation was disclosed when the particle diameters exceed 60 nm as the scattering dominates the absorption. Results revealed that he particle diameter can change the maximum temperature as well as the heat distribution in the surrounding medium. Particles in the range 20-40 nm produce sharp thermal concentration, which is localized at the surface interface (<10 nm from the surface). The larger particles (>40 nm) exhibit a unique phenomenon (secondary hot spots) at the far-field range, which extends the effective thermal range in the catalyst. Finally, the reaction rate constant does not continuously increase with decreasing the particle diameter as a precise balance between the surface-to-volume ratio and photothermal conversion efficiency, whose maximum was obtained for the particle diameter of 40 nm.

Keywords: Nanoparticles; Plasmonic resonance; Photothermal conversion; Secondary hot spots
Received: September 2025; **Revised:** November 2025; **Accepted:** December 2025; **Published:** January 2026

1. Introduction

The study of photothermal catalysis starts from the deep understanding of the radiation-matter interaction in the nanoscale. In noble metals, such as gold and silver, shifting a cloud of free electrons with respect to its stable ionic network leads to generate a Coulomb restoring force, which creates a resonance oscillation known as localized surface plasmon resonance (LSPR) [1,2]. This resonance is an optical phenomenon as well as a process of concentrating huge energy that compresses the incident light wavelength to nanoscale dimensions, which leads to a near-field enhancement of several orders of magnitude at the edges of the nanostructure [3,4]. Theoretically, this phenomenon can be described by the polarization equation of spherical particles within the dipole approximation where the electrical permittivities of the metal and surrounding medium play crucial role in determining the resonance frequency [5,6]. The capability of such nanostructures to operate as nano-antennas allows to absorb photons more than their geometrical cross section area, which establishes the primary fundamental of converting the light energy into chemical and thermal energies and hence overcome the conventional absorption limits in semiconductors and provide a unique platform for the molecular reactions throughout the direct excitation of the chemical bonds adsorbed on the surface [7-9].

The plasmon enters in a series of decays as soon as been excited and these decays occur at ultrashort time durations starting with the radiative decay or nonradiative decay via a mechanism known as Landau damping [10,11]. In the nonradiative damping, the plasmon energy transfers within femtoseconds to individual electrons producing hot charge carriers with high kinetic energies exceeding fermi level. These hot charge carriers can migrate to the lower unoccupied molecular orbitals (LUMO) to initiate photochemical reactions or they are subjected to dispersion (electron-electron or phonon-electron), which leads at the end to convert their energy to substantial heat increasing the temperatures of the nanostructure and its surrounding [12-14].

The research challenge in photothermal catalysis lies in the distinguishing between the macroscopic thermal effect, resulted from increasing the overall temperature, and the local nanothermal effect, which is also known as the hot spots [15-17]. Recent studies showed that the heat generated on the nanoparticle surface can reach to a critical values sufficient to break the stable covalent bonds, such as

N=N and C-H, under moderate illumination conditions, which makes this technique very useful in decreasing the carbon footprint of the industrial processes [18-20].

The variable size of the nanostructure represents the most effective parameter in determining the dominant pathway of heat dissipation because it works as a tuning switch of the photothermal conversion efficiency [21]. In the ultra-small particles (<10-20nm), the Landau damping rate increases due to increasing electronic collisions with the surface, which enhances the production of hot charge carriers and makes the absorption is the dominant phenomenon over the scattering. However, the low heat capacity of these particles means they cool down very fast, which requires high light density to maintain the surface temperature [22-24]. On the other hand, the larger particles (>50nm) show higher scattering that reduces the overall absorption efficiency per unit volume. Though, these particles have a surface area large enough to absorb maximum heat flows and distribute them differently within the medium [25,26]. The transformation from classical scale to quantum scale changes the function of the absorption cross-section as the surface-to-volume ratio becomes crucial in the determination of the number of active sites available for catalysis. Therefore, understanding the quantum relationship between the diameter and heat generation rate is important to design catalysts that avoid energy waste and ensure sustainable catalysis process [27,28].

Moving photothermal catalysis from laboratory of industrial environment needs to overcome the problems of nanoscale thermometry as the heat in the nanoscale does not necessarily obey the classical laws of thermal conductivity (Fourier's law) because the mean free path of phonons may be larger than the particle geometry and hence may lead to the appearance of Kapitza resistance, which limits the heat transfer to the solvent or substrate [29]. Contemporary research works focus on the development of mathematical models combining Maxwell's equations of electromagnetic fields with the heat transfer equations in porous media, considering the size-dependent prediction of the catalyst behavior under harsh operation conditions [30]. As well, combining physical concepts with surface chemistry opens the gate to design reactors working under the direct sunlight to invest the whole solar spectrum (from Uv to IR) by mixing nanostructures of various sizes. The final goal is to achieve a smart catalysis system that is able to guide the energy at molecular accuracy in order to reduce the side reactions and enhance the catalysis life by avoiding the unnecessary overall heating, which represents the innovative core of modern green chemistry [31,32].

2. Experimental Part

A precise computer model was developed to depend on the finite-domain time differences (FDTD) technique using ANSYS Lumerical software to explore the optical interaction between the incident light and metallic nanostructures of various sizes. The simulation environment was designed by construction of a 3D space surrounded by a completely absorbing layers to prevent the artificial reflections at the interfaces and a TFSF light source was incorporated to simulate the concentrated solar radiation. The optical characteristics of the gold and silver was ascribed to the Drude-Lorentz model to ensure real frequency response. A comprehensive parametric scan was performed to the geometrical diameters ranging from 10 to 100 nm with an increment of 5 nm. The calculations have focused on the extraction of the absorption and scattering cross sections (σ_{abs} and σ_{scat}) together with a near-field supportive analysis around the particles. A high-accuracy calculation mesh (0.5 nm) at the interface between metal and surrounding medium to guarantee the accurate calculation of energy flows and heat resulted from the Ohmic losses, which are mathematically represented by the volume dissipating power density as:

$$Q(r) = \frac{1}{2} Re\{J^*.E\} \quad (1)$$

This stage provides a digital database to predict the plasmonic behavior before transforming to the thermal stage, which enables to determine the sizes that achieve the maximum efficiency of energy absorption.

In the next step, the results of volumetric heat generation obtained from ANSYS Lumerical to COMSOL Multiphysics environment using a heat transfer unit in solids and liquids. This step depends on the formulation of the following transient heat equation:

$$Q = \nabla(-k\nabla T) + \rho c_p \frac{\partial T}{\partial t} \quad (2)$$

Where the temperature-dependent theromphysical properties were defined for both nanoparticle and the surrounding medium (catalyst solution). The experimental methodology has considered the Kapitza resistance at the interface between the nanoparticle and the medium, which is a critical parameter determining the heat transfer rate from the metallic surface to the reactive molecules. The time required to reach the steady state was simulated with monitoring the formation of hot spots around the particles

of various sizes. The recorded results showed that the smaller particles (<20 nm) produced local thermal gradient much sharper than the larger particles despite that the overall absorbed energy was lower. This confirms that the photothermal conversion efficiency does not relate only to the amount of absorbed light but also to how this energy is dissipated at the nanoscale. This multiphysical simulation allowed to configure a precise thermal map combining the particle diameter with the maximum temperature to be achieved on the catalyst surface.

The final step of the experimental work was a series of laboratory experiments to verify the validity of the computer models as plasmonic nanoparticles were prepared with controlled sizes using the wet chemical reduction method. The prepared nanoparticles were characterized to confirm the accuracy of their diameters. The UV-visible spectrophotometry was used to compare the peaks of the plasmonic resonance with the results of the simulation. In order to evaluate the photothermal catalysis, the samples were placed inside a dark reactor supplied with a light source simulating the solar radiation (AM1.5G) and a typical reaction (such as 4-nitrophenol) was used as a standard to measure the chemical activity. The reaction rate was recorded by measuring the change in absorbance over time whereas the overall solution temperature was recorded using IR cameras. The experimental results revealed an observed agreement with the theoretical predictions and the analytical part indicated that the moderate particles (about 40 nm) have achieved an ideal balance between the catalyst stability and energy conversion efficiency. The modified Arrhenius equation was applied to relate the increase in the reaction rate constant (k) to the local increase in temperature that confirmed that the nano-photothermal effect was the primary motivate to exceed the activation energy barriers and hence pave the way to design sustainable catalysis systems totally depend on the local solar energy.

3. Results and Discussion

Figure (1) shows the absorption cross section versus scattering cross section for the plasmonic nanoparticles. The triangle curve represents the absorption cross section (σ_{abs}), i.e., the ability of the particle to convert the light energy into thermal energy, while the circle curve represents the scattering cross section (σ_{scat}), i.e., the ability of the particle to re-direct the light energy in different directions. Specific values of diameters (20, 40, 60, and 100 nm) were considered to introduce the effect of particle size. Both curves show overall – but different – increase in the cross-sectional area with increasing nanoparticle diameter. This increase is a direct result to increase particle size and hence increase the number of conduction electrons contributing to the collective plasmonic oscillation as well as increase the surface area exposed to incident photons.

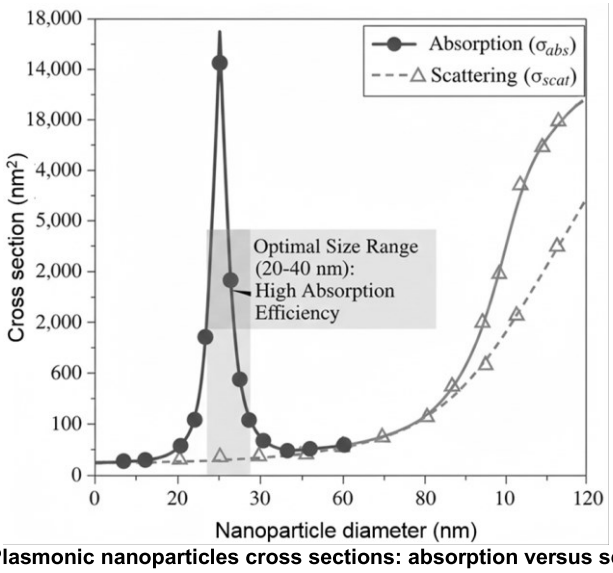

Fig. (1) Plasmonic nanoparticles cross sections: absorption versus scattering

At small diameters (<20 nm), the absorption clearly dominates the scattering, which is theoretically expected behavior throughout the quasi-static approximation as the particle size is reasonably smaller than the light wavelength. In such system, the dissipation due to the collisions of electrons with particle walls is the dominant (landau damping). This converts the plasmon energy into heat. This feature is

necessary for the photothermal therapy of cancer cells as an effective conversion of light energy into localized heat is required.

In the diameter range of 20-40 nm, results showed that the absorption reaches high efficiency, therefore, this range can be considered as the optimum size range, within which the absorption still dominant but the contribution of the scattering observably started. This range is optimum for many hybrid theranostic applications combining the heat generation (treatment) and detectable scattering signal (imaging). At the larger sizes (>40 nm), the circle curve exceeds the triangle curve gradually then abruptly. This is attributed to the fact the larger particles work as nanoantennas with higher efficiency. With increasing diameter, the dependency of the plasmonic response on the spatial phase of electric field to the incident light becomes high (out of the approximation of steady state), which enhances the re-emission. The scattering efficiency reaches its maximum at diameters of 100 nm or larger that makes these particles optimum for the applications of metal-enhanced fluorescence (MEF) and surface-enhanced Raman scattering (SERS). It is observed that the scattering curves is much more gradient than the absorption curve (i.e., higher sensitive to variable size). This is attributed to the fact that the scattering cross section approximately proportional to R^6, where R is the particle radius, within the resonance range, while the absorption cross section is proportional to R^3. Consequently, doubling the particle diameter may lead to a slight increase in the absorbance but a huge increase in scattering intensity, as can be shown by the expanding gap between the two curves beyond diameter of 60 nm.

Figure (2) shows the variation of temperature difference with the distance from nanoparticle surface. This complex thermal behavior relates the difference in the localized surrounding temperature (ΔT) to the vertical distance from the nanoparticle surface. It is classified into three main types based on the particle diameter. For particle diameters of 20-40 nm, a very sharp thermal response is observed directly on the surface as the difference in temperature reaches its peak (over 120°C) at zero distance then a fast exponential decay is observed and the thermal effect is completely vanished at distance of 10 nm. This refers to a high heat concertation in the directly adjacent layer to the surface (interface). This is ascribed to the high optical absorption efficiency as well as high surface energy flow density for these diameters.

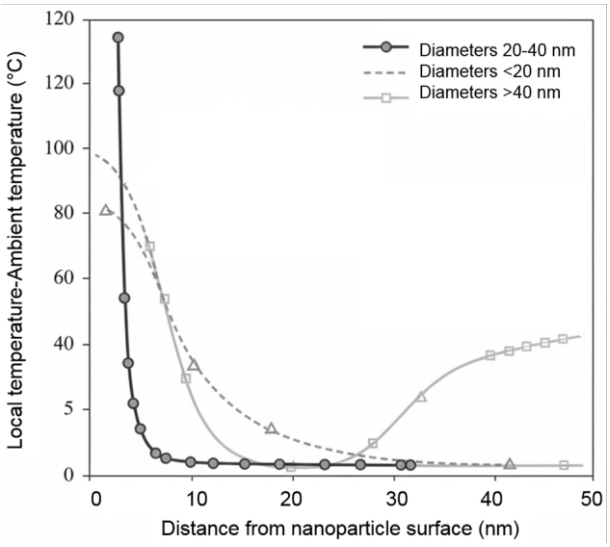

Fig. (2) Variation of temperature difference with the distance from nanoparticle surface

For particles smaller than 20 nm, the behavior looks much more moderate at the surface (starting from 100°C) with a slower thermal gradient extending to larger distances (up to 30 nm before steady state). This behavior is attributed to the effect of increasing the surface-to-volume ratio that enhances the heat dissipation in the surrounding medium instead of concentrating it in specific point. For diameters larger than 40 nm, the behavior is interestingly different with the existence of distinct secondary hot spots away from the surface. After fast and initial thermal reduction, a gradual increase starts beyond 30 nm to reach a new thermal stability at relatively high levels (about 40°C). This phenomenon is interpreted by the optical interference or plasmonic resonance as the heat may be generated at the far-field regions due to the intense scattering of light around these large particles. Such reasonable contrast

 ISSN (print) 2958-8960 (online) 3006-6042 Printed in IRAQ

in the thermal distribution patterns reveals that the control of nanoparticle diameter can change the maximum temperature and re-configure the thermal envelope surrounding the particle. This has crucial applications in hyperthermia to treat cancer as well as the phototherochemical reactions as the efficiency depends on the particle's temperature and the range to which the thermal effect can reach in the surrounding biological or chemical environment.

Figure (3) shows the variation of reaction rate constant with nanoparticle diameter. This dynamic relationship between the nanoparticle diameter and reaction rate constant refers to the size-dependent nature of the catalysis or chemical activity at the nanoscale. Analytically, the curve shows nonlinear behavior with a clear optimum point. The reaction starts with a relatively low rate for the smaller particles (10 nm) then steadily and rapidly increases with increasing the diameter to reach the maximum efficiency at diameter of about 40 nm as the reaction rate constant is 90 1/s. This initial jump is interpreted due to surface chemistry as an ideal number of the active sites are available and they are geometrically and electronically compatible with the reactive molecules at this specific diameter. However, as soon as this critical threshold is exceeded (40 nm), a gradual and uniform decrease in the reaction rate constant is observed with increasing particle diameter to reach its minimum at 100 nm (~30 1/s). This retraction is attributed to the reduced surface-to-volume ratio, as the number of atoms on the surface is decreased with increasing particle diameter when compared to the overall volume. This in turn reduces the effective collisions and chemical bonding. The degraded performance at large diameters may also be ascribed to the variations in the electronic characteristics and surface charge distribution, or to the mass transfer limitations that become much more apparent with increasing catalyst particle diameter. The existence of this sharp peak clearly refers to the chemical activity of this system, which not always follows the principle of "the smallest is the best", but obeys the phenomena of quantum confinement and surface tension effects. This makes the range of 35-45 nm is the best criterion to achieve the maximum reactivity and hence provide results for the design of precisely-engineered nanocatalysts for industrial and biomedical applications.

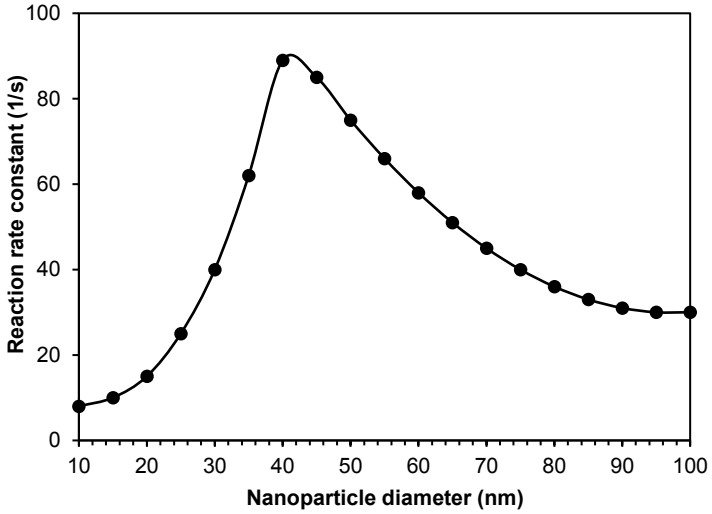

Fig. (3) Variation of reaction rate constant with nanoparticle diameter

4. Conclusions

In concluding remarks, a tight and nonlinear relation between particle diameter and optical properties was confirmed as the particles with diameters in the range 25-35 nm have achieved the maximum efficiency of light absorption, making this range optimum to convert the photons into condensed local heat. A radical transformation was disclosed when the particle diameters exceed 60 nm as the scattering dominates the absorption. Results revealed that he particle diameter can change the maximum temperature as well as the heat distribution in the surrounding medium. Particles in the range 20-40 nm produce sharp thermal concentration, which is localized at the surface interface (<10 nm from the surface). The larger particles (>40 nm) exhibit a unique phenomenon (secondary hot spots) at the far-field range, which extends the effective thermal range in the catalyst. Finally, the reaction rate constant does not continuously increase with decreasing the particle diameter as a precise balance between the

surface-to-volume ratio and photothermal conversion efficiency, whose maximum was obtained for the particle diameter of 40 nm.

References

[1] A. V. Tumarkin et al., "Preparation of alumina thin films by reactive modulated pulsed power magnetron sputtering with millisecond pulses", *Coatings*, 14(1) (2024) 82.
[2] A.N. Munif and F.J. Kadhim, "Structural Characteristics and Photocatalytic activity of TiO2/Si3N4 nanocomposite synthesized via plasma sputtering technique", *Iraqi J. Phys.*, 22(4) (2024) 99-106.
[3] A.Y. Bahlool, "Temperature-Dependent Optoelectronic Characteristics of p-SnO_2/n-Si Heterojunction Structures", *Iraqi J. Appl. Phys. Lett.*, 7(1) (2024) 23-26.
[4] B.K. Nasser and M.A. Hameed, "Structural Characteristics of Silicon Nitride Nanostructures Synthesized by DC Reactive Magnetron Sputtering", *Iraqi J. Appl. Phys.*, 15(4) (2019) 33-36.
[5] D. Mattox, **"Handbook of Physical Vapor Deposition (PVD) Processing"**, 2nd ed., Ch. 7, William Andrew, (Amsterdam, 2010).
[6] D.A. Taher and M.A. Hameed, "Employment of Silicon Nitride Films Prepared by DC Reactive Sputtering Technique for Ion Release Applications", *Iraqi J. Phys.*, 21(3) (2023) 33-40.
[7] D.A. Taher and M.A. Hameed, "Structural and Hardness Characteristics of Silicon Nitride Thin Films Deposited on Metallic Substrates by DC Reactive Sputtering Technique", *Silicon*, 15 (2023) 7855-7864.
[8] E. Kianfar and V. Cao, "Polymeric membranes on base of PolyMethyl methacrylate for air separation: a review", *J. Mater. Res. Technol.*, 10 (2021) 1437-1461.
[9] F.J. Al-Maliki et al., "Optimization of Rutile/Anatase Ratio in Titanium Dioxide Nanostructures prepared by DC Magnetron Sputtering Technique", *Iraqi J. Sci.*, 60(special issue) (2019) 91-98.
[10] F.J. Kadhim et al., "Fabrication of UV Photodetector from Nickel Oxide Nanoparticles Deposited on Silicon Substrate by Closed-Field Unbalanced Dual Magnetron Sputtering Techniques", *Opt. Quantum Electron.*, 47(12) (2015) 3805-3813.
[11] K. Seshan, **"Handbook of Thin Film Deposition: Techniques, Processes, and Technologies"**, 3rd ed., Ch. 4, William Andrew (Amsterdam, 2012).
[12] K.A. Al-Hamdani, "Current–voltage and capacitance-voltage characteristics of Se/Si heterojunction prepared by DC planar magnetron sputtering technique", *Iraqi J. Phys.*, 8(13) (2010) 97-100.
[13] M. Said et al., "Microwave hybrid heating for lead-free solder: A review", *J. Mater. Res. Technol.,* 26 (2023) 6220-6243.
[14] M.A. Hameed and Z.M. Jabbar, "Preparation and Characterization of Silicon Dioxide Nanostructures by DC Reactive Closed-Field Unbalanced Magnetron Sputtering", *Iraqi J. Appl. Phys.*, 12(4) (2016) 13-18.
[15] M.K. Khalaf et al., "Fabrication and Characterization of UV Photodetectors Based on Silicon Nitride Nanostructures Prepared by Magnetron Sputtering", *Proc. IMechE, Part N, J. Nanomater. Nanoeng. Nanosys.*, 230(1) (2016) 32-36.
[16] M.K. Khalaf et al., "Operation Characteristics of a Closed-Field Unbalanced Dual-Magnetrons Plasma Sputtering System", *Bulg. J. Phys.*, 41(1) (2014) 24-33.
[17] M.S. Edan, "Copper Nitride Nanostructures Prepared by Reactive Plasma Sputtering Technique", *Iraqi J. Mater.*, 4(1) (2025) 31-36.
[18] N.A.H. Hashim and F.J. Kadhim, "Structural and Optical Characteristics of Co_3O_4 Nanostructures Prepared by DC Reactive Magnetron Sputtering", *Iraqi J. Appl. Phys.*, 18(4) (2022) 31-36.
[19] O.A. Hammadi, "Nanostructured CdSnSe Thin Films Prepared by DC Plasma Sputtering of Thermally Casted Targets", *Iraqi J. Appl. Phys.*, 14(4) (2018) 33-36.
[20] P.M. Martin, **"Introduction to Surface Engineering and Functionally Engineered Materials"**, Ch. 6, John Wiley & Sons (NJ, 2011), p. 339.
[21] R.A. Anaee et al., "Alumina Nanoparticle/Polypyrrole Coating for Carbon Steel Protection in Simulated Soil Solution", *Eng. Tech. J.*, 35(9A) (2017) 943-949.
[22] R.H. Turki and M.A. Hameed, "Spectral and Electrical Characteristics of Nanostructured NiO/TiO_2 Heterojunction Fabricated by DC Reactive Magnetron Sputtering", *Iraqi J. Appl. Phys.*, 16(3) (2020) 39-42.
[23] S.U. Ilyasa, R. Pendyalaa, and N. Marneni, "Stability and Agglomeration of Alumina Nanoparticles in Ethanol-Water Mixtures", *Procedia Eng.*, 148 (2016) 290-297.
[24] Y. Zhang et al., "A review paper on effect of the welding process of ceramics and metals", *J. Mater. Res. Technol.*, 9(6) (2020) 16214-16236.
[25] A.M. Hameed and M.A. Hameed, "Spectroscopic characteristics of highly pure metal oxide nanostructures prepared by DC reactive magnetron sputtering technique", *Emerg. Mater.*, 6 (2022) 627-633.
[26] A.S. Reddy, H.-H. Park and V.S. Reddy, "Effect of sputtering power on the physical properties of dc magnetron sputtered copper oxide thin films", *Mater. Chem. Phys.*, 110(2-3) (2008) 397-401.
[27] C. Otero et al., "Optoelectronic Response of Multilayer CuO/NiO Nanostructures Fabricated with Different Particle Size Ranges", *Iraqi J. Appl. Phys. Lett.*, 8(1) (2025) 29-32.
[28] D.A. Taher and M.A. Hameed, "Spectroscopic Characteristics of Silicon Nitride Thin Films Prepared by DC Reactive Sputtering Using Silicon targets with Different Types of Conductivity", *Iraqi J. Appl. Phys.*, 19(4A) (2023) 73-76.
[29] F.J. Al-Maliki and E.A. Al-Oubidy, "Effect of gas mixing ratio on structural characteristics of titanium dioxide nanostructures synthesized by DC reactive magnetron sputtering", *Physica B: Cond. Matter*, 555 (2019) 18-20
[30] K.A. Aadim, "Control the deposition uniformity using ring cathode by DC discharge technique", *Iraqi J. Phys.*, 15(32) (2017) 57-60.
[31] M.A. Hameed et al., "Characterization of Multilayer Highly-Pure Metal Oxide Structures Prepared by DC Reactive Magnetron Sputtering Technique", *Iraqi J. Appl. Phys.*, 16(4) (2020) 25-30
[32] S.H. Faisal and M.A. Hameed, "Heterojunction Solar Cell Based on Highly-Pure Nanopowders Prepared by DC Reactive Magnetron Sputtering", *Iraqi J. Appl. Phys.*, 16(3) (2020) 27-32.

